Redox Biology 19 (2018) 210–217

Contents lists available at ScienceDirect

Redox Biology

journal homepage: www.elsevier.com/locate/redox

Research paper

Co-imaging extrinsic, intrinsic and effector caspase activity by fluorescence anisotropy microscopy

Agustin A. Corbat[a,1], Klaus C. Schuermann[b,1], Piotr Liguzinski[b], Yvonne Radon[b], Philippe I.H. Bastiaens[b], Peter J. Verveer[b,*], Hernán E. Grecco[a,b,**]

[a] Department of Physics, FCEN, University of Buenos Aires and IFIBA, CONICET, Buenos Aires, Argentina
[b] Department of Systemic Cell Biology, Max Planck Institute of Molecular Physiology, Dortmund, Germany

ARTICLE INFO

Keywords:
Caspase activity
Apoptotic network
Anisotropy FRET biosensor
Co-monitoring
Imaging
Polarization microscopy

ABSTRACT

In order to overcome intercellular variability and thereby effectively assess signal propagation in biological networks it is imperative to simultaneously quantify multiple biological observables in single living cells. While fluorescent biosensors have been the tool of choice to monitor the dynamics of protein interaction and enzymatic activity, co-measuring more than two of them has proven challenging. In this work, we designed three spectrally separated anisotropy-based Förster Resonant Energy Transfer (FRET) biosensors to overcome this difficulty. We demonstrate this principle by monitoring the activation of extrinsic, intrinsic and effector caspases upon apoptotic stimulus. Together with modelling and simulations we show that time of maximum activity for each caspase can be derived from the anisotropy of the corresponding biosensor. Such measurements correlate relative activation times and refine existing models of biological signalling networks, providing valuable insight into signal propagation.

1. Introduction

Cellular function emerges from the concerted activities of multiple proteins structuring interconnected signalling networks that receive, process and relay information. To understand signal propagation and thereby cellular processes it is necessary to monitor the state of key nodes in such networks with high spatial and temporal resolution in single living cells [42,40]. The aforesaid comprehension of information flow and regulation between key nodes has brought insight in therapy development [27].

One of such networks is the apoptotic signalling cascade. The apoptotic network can be portrayed by describing the activation dynamics of its key nodes which are the proteases known as caspases. These are cysteine-aspartic proteases found in animal cells as inactive proenzymes, which can be classified into effector caspases, capable of directly dismantling cells, and initiator caspases, regulating effector caspases [2]. Initiator caspases can be further classified into extrinsic or intrinsic whether they transduce signalling from ligands, such as TNF-α, or from inside the cell, such as reactive oxygen species or DNA damage [29]. Quantifying the activation timing between caspases could provide information about the network topology and connection strength.

Fluorescent biosensors have long been the tool of choice to obtain time courses of the single cell state of these nodes [12]. In particular, ratiometric Förster Resonant Energy Transfer (FRET) based approaches using fluorescent proteins (FP) have provided dynamical information with subcellular resolution [30,8]. FRET is the non-radiative energy transfer, via dipole-dipole coupling, between two nearby (~5 nm) fluorophores. The energy transfer rate is dependent on the relative distance and orientation of the fluorophores and thereby is a sensitive readout of the biosensor conformation.

A typical ratiometric heteroFRET biosensor consists of two spectrally separated fluorophores: a donor and a red-shifted acceptor. These are usually linked by a sensitive domain that transduces a biological signal, for example phosphorylation [25,11], methylation [19,15] or protein cleavage [41], to a conformational change which can be measured as a variation in the relative donor/acceptor fluorescence intensity.

Several reports demonstrated simultaneous imaging of two different ratiometric FRET sensors [1,26,22,24,9,23,18,21]. However, due to the broad spectra of FP it is challenging to image more than 2 sensors (4 FP) in the visible range. When cellular compartments of interest can be spatially resolved, sensors with similar spectral properties can be

* Corresponding author.
** Corresponding author at: Department of Physics, FCEN, University of Buenos Aires and IFIBA, CONICET, Buenos Aires, Argentina.
E-mail addresses: pjverveer@gmail.com (P.J. Verveer), hgrecco@df.uba.ar (H.E. Grecco).
[1] Both authors contributed equally to this work.

https://doi.org/10.1016/j.redox.2018.07.023
Received 28 June 2018; Received in revised form 23 July 2018; Accepted 31 July 2018
Available online 09 August 2018

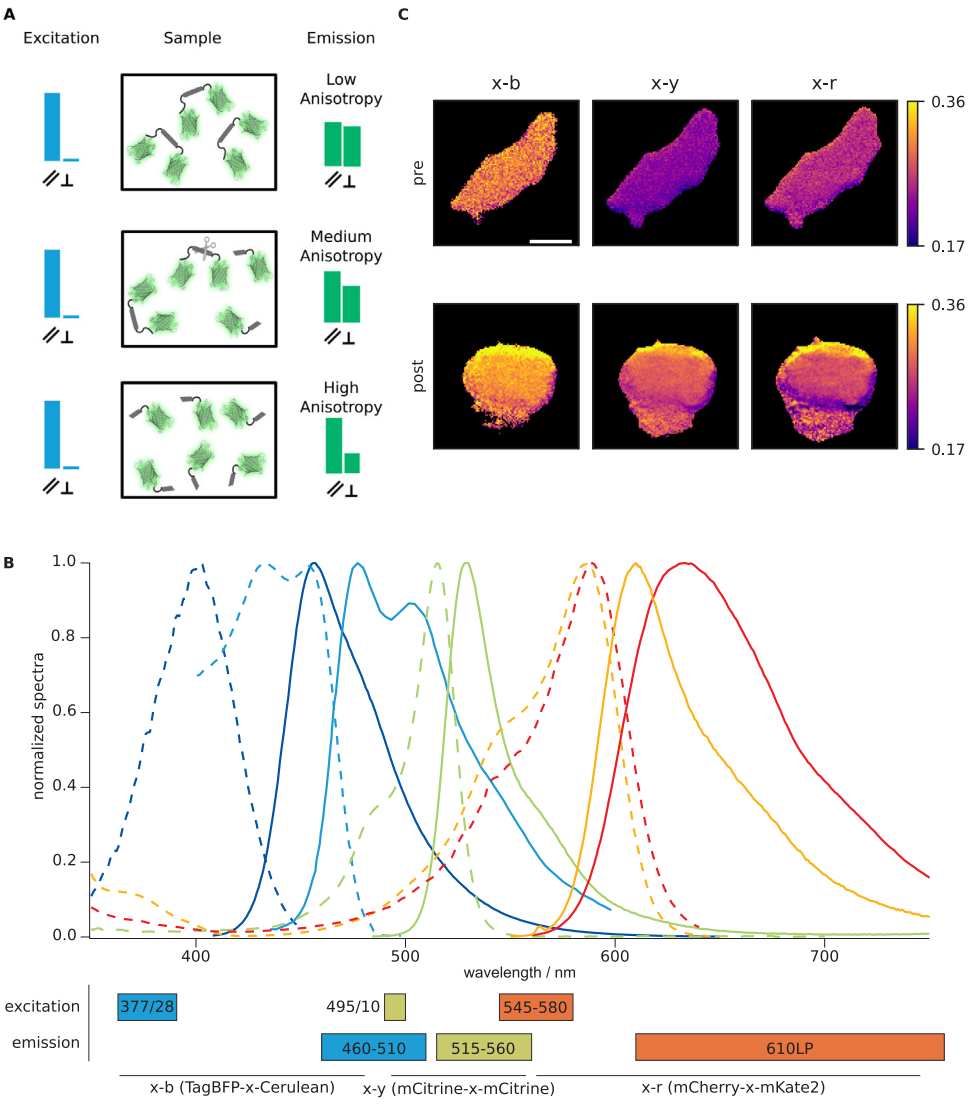

Fig. 1. Spectrally separable anisotropy FRET-based sensors state can be determined by fluorescence polarization microscopy. (A) Fluorescent proteins within a sensor are linked by a sequence recognized by the protease of interest. Upon activation of this enzyme, the population of sensors is gradually cleaved. Consequent to excitation with linearly polarized light, the emission of the ensemble of fluorescent proteins exhibits a significant polarization anisotropy due to the occurrence of FRET in dimers. In contrast, as dimers are cleaved into monomeric state, the emission of fluorescent proteins is more polarized. As the reaction is unidirectional, the fraction of cleaved sensor is therefore a measure of the integral activity of the protein of interest. (B) Excitation and emission spectra of FRET sensors designed to take advantage of the visible range in order to monitor simultaneously the activity of three enzymes. Filters used to visualize each fluorophore are detailed below the plot. (C) Anisotropy images obtained for a single cell where each column corresponds to each channel. The same cell was imaged before and after apoptosis and is shown in each row. A considerable change in anisotropy can be appreciated in each channel along with typical apoptotic morphological changes. Scale bar is 10 μm.

targeted to each of them; a technique known as spatial multiplexing [10,26,13]. In other cases, computational multiplexing (i.e. to digitally combine the information from multiple cells expressing different pairs of sensors) has also been used to co-measure three sensors [22]. However, the applicability is limited due to high variability in biological systems. It would be desirable to have a FRET sensor with a narrower spectra in order to image more activities simultaneously.

FRET between identical or spectrally similar fluorescent proteins can also be measured by monitoring the depolarization of the emission using fluorescence polarization microscopy, and has the advantage of reducing spectra per sensor. Upon excitation with linearly polarized light, the fluorescence emission of FP will be anisotropic due to a photoselection effect on fluorophores and a large rotational diffusion time as compared to the fluorescence lifetime. To the contrary, FRET will transfer energy to non-photoselected FP resulting in a more isotropic emission [6,28]. This can be determined by comparing the polarization components in the planes parallel and perpendicular to the excitation (see Fig. 1A). Genetically encoded proteins have been designed to implement this technique for detection of protein clustering [5], measuring protein conformations [37] and protease activity [33]. Unlike their heteroFRET counterparts in which analytical methods to derive quantitative biological information have been broadly demonstrated [31], information derived from anisotropy FRET-based sensors has mostly remained at the qualitative level. However, it is of interest to pursue this family of biosensors as their narrower spectral window per sensor would in principle allow to co-measure a larger number of them [32]. Until now, only two number of activities have been co-measured [39].

In this work we demonstrate for the first time that three biosensors can be indeed co-measured and also provide a quantitative and reliable readout of the timing of key events in a signalling network. We apply this concept to track in time three key steps in the apoptotic network, namely the activation of caspase 8, 9 and 3 (extrinsic, intrinsic and effector caspases respectively). Our results demonstrate that multiparametric quantification allows to distinguish between competing molecular models and therefore provide a more detailed insight into signal propagation.

2. Results

2.1. Design of three spectrally separable FRET based biosensors

We designed and optimized three spectrally distinct anisotropy FRET-based biosensors. For this purpose we calculated the Förster radii of different pairs of fluorescent proteins with suitable spectral characteristics. We generated several candidate tandem constructs across the visible spectrum for those with larger R_0 and compared their fluorescence anisotropy to their single FP counterpart (Supplementary Fig. 1). It is worth noticing that in the blue range, constructs consisting of different kinds of FP were looked into due to their short Förster

distance. Here, the difference in anisotropy between states arise not only from FRET but also from the filters used and the effect of objectives NA [32]. The same approach was found useful in the red range.

Some of the tandem constructs showed a significant anisotropy change indicating the occurrence of FRET. On the other hand, some constructs did not exhibit a significantly lower fluorescence anisotropy than their monomer counterpart most likely due to an unfavourable relative orientation of the chromophores in the constructs, an effect that is difficult to take into account in the calculations of Förster distance. Among those, we selected a set of three constructs and their corresponding filters that could be co-expressed and imaged simultaneously in the same cell. The selected sensor set consisted of TagBFP-x-Cerulean (named here: x-b), mCitrine-x-mCitrine (x-y) and mCherry-x-mKate2 (x-r) (Fig. 1B).

Having successfully obtained a suitable sensor set, we engineered each of them into a caspase activity sensor by replacing the linker (x) with a cleavable sequence specific for caspase 3 (Cas3). HeLa cells were transfected with these sensors (Cas3-b, Cas3-r and Cas3-y) and subjected to an apoptotic stimulus leading to caspase activation and subsequent biosensor cleavage (See Section 4.2). Using automated fluorescence microscopy, modified for polarization fluorescence measurements, we monitored the state of the sensor set. Resulting images were background and G-factor corrected and segmented into individual cells (see Supplementary Fig. 2 and Sections 4.3 and 4.4). This procedure resulted in a significant change in their polarization anisotropy confirming the expected biosensor function (Fig. 1C).

2.2. From anisotropy signal to enzymatic activity

As onset of apoptosis can occur anytime during the length of the experiment, sensors were monitored before, during and after the outstart. The mean anisotropy and intensity among other estimators together with morphological attributes were calculated for the cell. Anisotropy change as well as morphological signs of apoptosis can be appreciated (see Fig. 2A).

The measured anisotropy at each time point reflects the mean anisotropy weighted by concentration of biosensor in each state (monomer vs dimer). Given that the cleavage reaction is unidirectional, the fraction of biosensor in monomeric, cleaved, state (m) results from the integrated enzymatic activity of the caspase of interest. It can be demonstrated from reaction equations and also numerically that the derivative of anisotropy time series, divided by the normalized anisotropy curve, is a good proxy of instantaneous caspase activity (see Section 4.5 and Fig. 2B and C). This holds true even for enzymes embedded in more complex networks.

To demonstrate this principle we modified a well established in silico model of the capase network [3] consisting in 58 species and 28 reactions by including the biosensors and simulated time evolution of the fraction of cleaved sensor from which the anisotropy was obtained (see Section 4.6). In this way we can compare the time of maximum activity (t_{max}) as obtained from simulations to the one derived from simulated anisotropy curve using the proposed method. Even for two distinct simulated activity profiles (see Fig. 2C red and blue) the time of maximum activity (dark arrow) agrees with the one derived by our method (dashed lines). In contrast, a common readout such as the time at which anisotropy reaches 50% of the change strongly depends on activity profile (blue and red stars).

2.3. Extrinsic, intrinsic and effector caspase activity were measured to study signal propagation in apoptotic network

In order to estimate the uncertainty of the method, anisotropy and corresponding caspase activity time series was obtained for each cell expressing three different spectral versions of caspase 3 activity sensors (Cas3-b, Cas3-r, Cas3-y, see Fig. 3A). All cells with a significant step increase in anisotropy exhibited the morphological changes expected for apoptosis. Time series corresponding to cells not responding to treatment were discarded (See Section 4.4). As expected, the observed transition of 54 different cells are scattered throughout the 15 h experiment (Fig. 3A rug plot) but the differences in activation time within the same cell was 1^{3}_{0} min. (median where lower and upper bounds correspond to the first and third quartiles, see Fig. 3B).

To investigate timing of the apoptotic network we then use the same principle to generate additional activity sensors for caspases 8 and 9 using previously published cleavage sequences (see Section 4.1) [41,36,35,16,7]. By co-transfecting Cas3-b, Cas8-r and Cas9-y in HeLa cells we measured the activation times of these key nodes in individual cells after stimulation with TNF-α (see Fig. 3C). While the activation time of effector caspase 3 was not deterministic after stimuli, caspase 3 always reached maximum activity before caspase 8 ($\Delta t = 5^{9}_{2}$ min.). This is consistent with the fact that caspase 8 activity grows slowly until caspase 3 feeds back into it (not shown) and with previously described models [20,3]. Furthermore, caspase 3 maximum activity preceded caspase 9 by 8^{14}_{5} min., meaning that caspase 9 was the last caspase to achieve maximum activity.

2.4. Correlation and distribution in measured timing deliver insight into apoptotic network modelling

Having observed simultaneously the three nodes of the network, a positive correlation was found between time difference from caspase 8 to caspase 3 (Δt (Cas3-b, Cas8-r)) and caspase 9 to caspase 3 (Δt (Cas3-b, Cas9-y), see Fig. 3D, orange contour). We hypothesized that the source of such heterogeneity might be cell to cell variability in the overexpressed sensor concentration and sequestration by the biosensor. To test this scenario in silico, we sampled biosensor initial concentration space and simulated time series to study caspase network timing using our adapted model (see Section 4.7).

We then applied the same analysis method that was used on experimental data to the simulated fluorescence anisotropy and found that variability in sensor expression significantly affected the timing between caspases and presented the same correlation. At a sensor concentration of 1.7μM, compatible with typical exogenous expression levels of FP in HeLa [38], and just 5–10 times higher than PARP concentration in the model, we could match the observed correlation of time. However, the distribution of time difference was not matched to the experimental data as is evident by the location of the distributions (Fig. 3D, purple vs orange contours).

Therefore, we seek out to modify the model conserving the observed experimental features in previous works but accounting from this novel correlative dataset. As stated previously by Albeck et al. in the original work presenting EARM [3], different stimuli will generate differences in the model at the level of ligand and receptor interaction. Therefore, we scanned parameters related to ligand and receptor activity. Reducing ligand concentration by a factor of 3 and increasing receptor concentration by 5 we could adequately describe timing between caspase 3 and caspase 8, but not caspase 9 (see Supplementary Fig. 3).

On the other hand, subsequent studies by Aldridge et al. [4] showed how different concentrations of XIAP relative to procaspase 3 give rise to different substrate cleavage profiles and types of apoptosis. We found that changes in the initial concentration of XIAP were sufficient to explain the differences in caspase maximum activity order of occurrence (see Fig. 3D, blue and E). This effect can be interpreted by noticing in the model that XIAP belongs to one of the pathways connecting caspase 8 with caspase 3, without going through caspase 9 (see Fig. 3D). To systematically obtain the optimal model values we scanned XIAP, ligand and receptor concentrations and compared the outcome of the simulation with our experimental results by comparing the time differences distributions (see Section 4.7, and Supplementary Fig. 4). Multivariate normal noise was added to simulated time differences using a covariance matrix calculated from the time differences distribution of the experiment where all linkers where specific for caspase

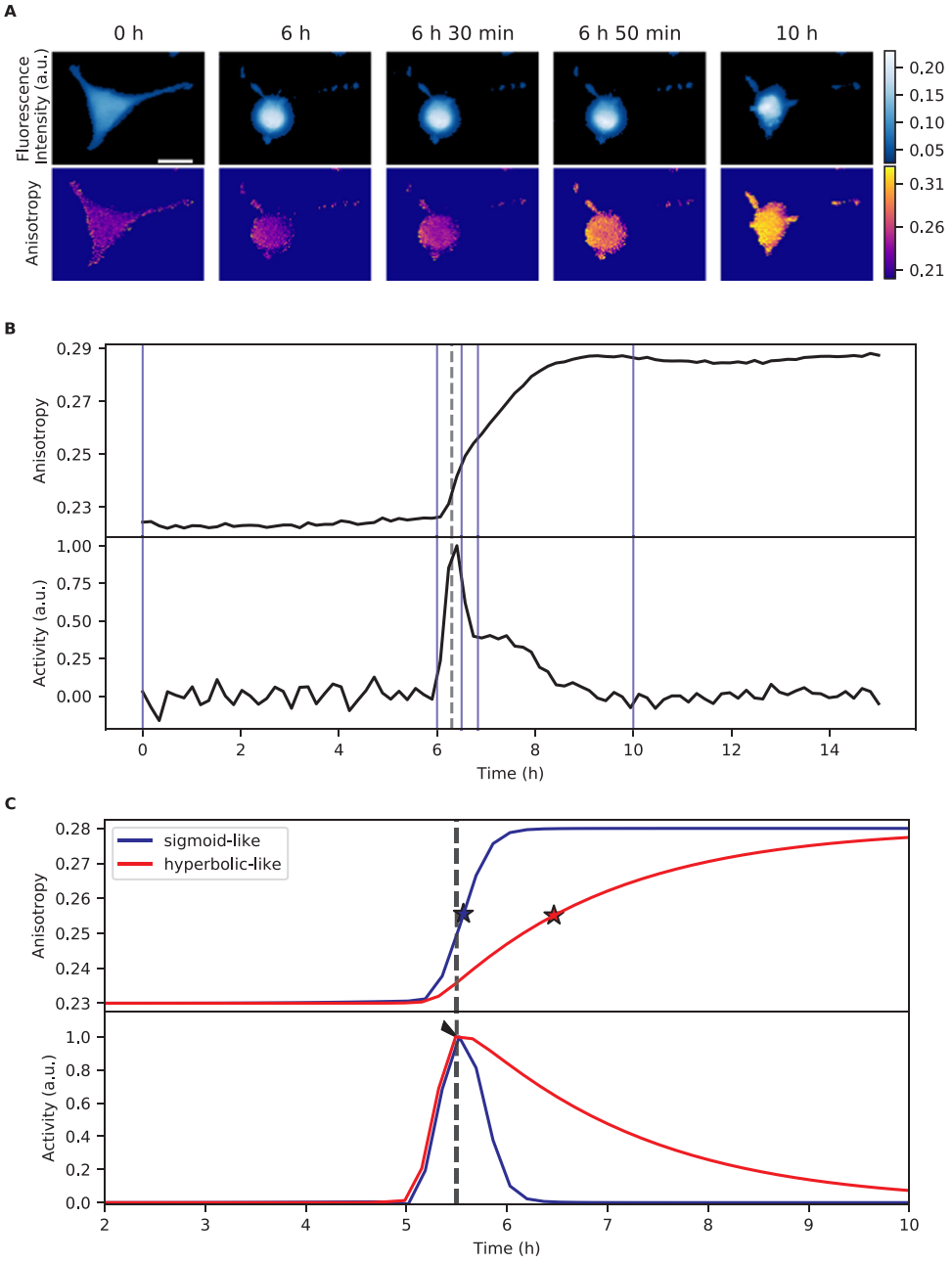

Fig. 2. Cells were transfected with the developed biosensors to transduce integral caspase activity into anisotropy signal. (A) Through fluorescence and fluorescence polarization microscopy we can see how apoptotic cells change their roundness and start blebbing, at the same time as we monitor the shift in anisotropy. Scale bar is 15 μm. (B) Anisotropy curve obtained from mean parallel and perpendicular intensity reports the integral activity of the caspase in study. Instantaneous enzymatic activity can be calculated after using finite differences to find the derivative of anisotropy. The time of maximum activity is a robust readout of caspase timing. Blue vertical lines represent the time from which images are shown. (C) By means of an adapted apoptotic network of ordinary differential equation model we simulated caspase activity over different concentrations of biosensors in the cell and the anisotropy signal detected. Sigmoid-like and hyperbolic-like profiles correspond to distinct possible enzymatic activities. Stars in anisotropy curves coincide with the time when anisotropy reaches 50% of total change. Using the described pipeline, it is clearly shown how simulated maximum activity (represented as a black arrow head) and t_{max} calculated from simulated anisotropy curve (dashed line) agree and do not depend on the signal profile, nor on the concentration of biosensor. (For interpretation of the references to color in this figure, the reader is referred to the web version of this article.)

3. By scanning these parameters we found that reducing XIAP concentration by three orders of magnitude exchanges the order between caspase 9 and caspase 3 to accurately describe experimental observations without affecting other predictions. Modifying ligand, receptor and XIAP initial concentration proved to be sufficient to recover our experimental observations without loosing any other previously observed predictions of the model.

3. Discussion

In this work we demonstrate for the first time that three anisotropy FRET-based biosensors can be co-measured in single cells obtaining correlative biological information from their photophysical signals. In this way, the propagation of biological signals in response to stimuli can be monitored by quantifying the state of key nodes within the network.

Our work introduces new options for imaging multiple signalling activities in single cells. Notably, the sensors are based on a broad palette of established fluorescent proteins, profiting from many years of optimization for cellular imaging purposes [34]. The acquisition of polarized imaging data can be achieved with relatively simple and inexpensive modifications of a standard fluorescence microscope. Anisotropy calculation is straightforward and relies on signal ratios, thus it is relatively insensitive to sample thickness, light intensity and concentration [14]. Therefore, the sensors presented in this work are in principle compatible with embryological and organotypic studies and could provide valuable insight about the spatial and temporal regulation of apoptosis during development and processes involved in neurodegeneration or neuronal loss.

Currently it is the only method capable of simultaneously imaging three FRET-based biosensors in a single cell without introducing additional limitations such as spatial or computational multiplexing. Moreover, simultaneous monitoring gives information on correlation between signals that would be otherwise missed out. Importantly, the principle is applicable to other readouts as long as a sensor motif is known.

Alongside the implementation of multiple sensor, our work reveals

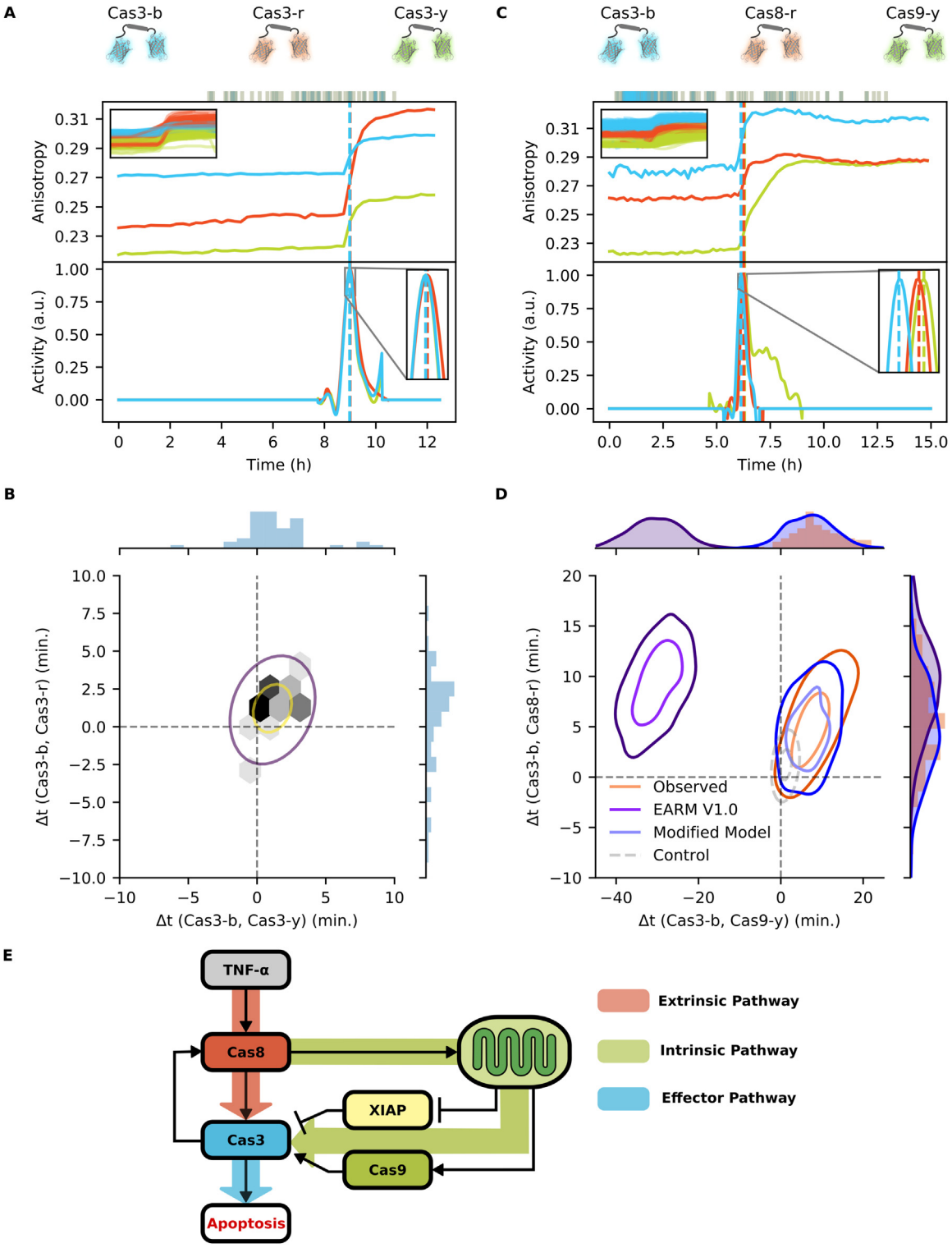

Fig. 3. Three spectrally distinct biosensors are used to analyze signal propagation in different nodes of a complex network. (A) Top panel: Anisotropy signal time series from three biosensors transducing activity of the same enzyme show similar behaviour. While the time of maximum activity differs substantially from cell to cell (rug plot, above), the variations between sensors within each cell is small. Inset: Time series for all cells (N = 54) time translated to maximum activity as reported by Cas3-b sensor (−2.5 to 2.5 h). Bottom panel: Proportional monomer derivative curve. Inset: zoom showing negligible time differences of maximum activity. (B) Bidimensional hexagonal histogram of time differences reported by Cas3-y (horizontal axis) and Cas3-r (vertical axis) referenced to Cas3-b (with histograms on respective axes). Kernel density contour lines enclosing 34% and 68% of data points. Notice that data points are concentrated near the origin. (C) Analogous to A where in this case anisotropy signals show the different activity profiles for caspase 8, 9 and 3 (N = 121 cells). Notice that significant time differences in activation are observed. (D) Orange contour lines represent experimental points meaning that caspase 3 maximum activity is reached first. Shown in Purple are results for a previously published model simulating the apoptotic network adapted only to include the biosensors without any parameter modification. While timing between caspase 3 and 8 are compatible, order and timing of caspase 9 does not coincide with observed timing. After modifying XIAP, ligand and receptor concentration, timing obtained through modelling is comparable to the one observed experimentally, shown in blue. (E) Simplified version of the apoptotic cascade model where main information flow routes are shown. (For interpretation of the references to color in this figure legend, the reader is referred to the web version of this article.)

novel analytical methods to transform photophysical signals corresponding to anisotropy experiments into the state of an enzyme of interest. From this biologically relevant readout, we derived the activation timing between effector and initiator caspases. In particular, we found effector caspase 3 reaches maximum activity 5^{9}_{2} minutes before extrinsic initiator caspase 8. Maximum activity of caspase 8 has been described to occur after caspase 3 due to its slow dynamics and feedback between them. Similarly, caspase 3 time of maximum activity takes place 8^{14}_{5} minutes before caspase 9 as XIAP inhibition from mitochondrial species is much faster than activation of caspase 9. Interestingly, XIAP initial concentration regulates whether cells go through type I or type II apoptosis, as previously stated.

Mathematical modelling was necessary to compare the specific order of activation, and the origin of the observed photophysical signal had to be interpreted as a result of the state of sensor ensemble and subsequently into active enzyme state. This procedure presents a complete process that is scalable to answer new biologically interesting questions. Other stimuli, such as reactive oxygen species could be used to onset an intrinsic apoptotic response and study differences in caspase activation order by perturbing the network at different nodes [33]. Through careful signal interpretation and data acquisition, biological networks can be simulated to better understand their systemic behaviors.

4. Methods

4.1. Plasmids

Anisotropy sensors were constructed by inserting a second fluorophore amplified by PCR and flanked by a SpeI and a SalI restriction site and containing a STOP codon into the SpeI/SalI restriction sites of a C1-vector backbone (Clontech). Additionally, the PCR product contained a short linker sequence at the 5′ end. These plasmids were used as non-cleavable controls. To construct the cleavable caspase sensors, the sequences encoding the cleavage sites of caspase 3, 8 and 9 (DEVD, IETD-IETD, LEHD, respectively) were amplified by PCR and the products, flanked by a BspI and a SpeI cleavage site, subcloned into the corresponding restriction sites of the digested non-cleavable control sensors. In addition, the PCR products were flanked by a previously published linker sequence [20].

4.2. Cell culture and imaging sample preparation

HeLa cells were grown in DMEM (PAN Biotech) supplemented with 10% fetal calf serum (FCS, Gibco), 100 U/ml penicillin, 100 µg/ml streptomycin, 1% L-glutamine and 1% non-essential amino-acids (all PAN Biotech) at 37 °C and 5% CO_2 in a humidified incubator. On the day before transfection cells were seeded in 8 well dishes (LabTekII, Nalgene) at a density of 3×10^4 cells. Transfection was carried out using Fugene 6 (Promega) following the manufacturer's protocol. 20 h post transfection cells were imaged in DMEM without Phenol red (PAN Biotech) and 0% FCS either in presence of 1 µM Staurosporin (Sigma Aldrich, Germany) or 50 ng/ml TNF-α (Invitrogen) together with 10 µg/ml Cycloheximide (Sigma Aldrich, Germany) to induce apoptosis or DMSO as a control.

4.3. Image acquisition

Data for anisotropy imaging was acquired with a custom built setup, as previously described [32,37]. Briefly, images were acquired using an Olympus IX81 inverted microscope (Olympus, Germany) equipped with a MT20 illumination system. A linear dichroic polarizer (Meadowlark Optics, Frederick, Colorado, US) was placed in the illumination path of the microscope, and two identical polarizers were placed in an external filter wheel at orientations parallel and perpendicular to the polarization of the excitation light. Fluorescence was collected via a 20X 0.7 NA air objective, and parallel and perpendicular polarized emission images were acquired sequentially on an Orca CCD camera (Hamamatsu Photonics, Japan). The CellR software (Olympus, Germany) or an in-house developed LabVIEW (National Instruments) program was used to control the data acquisition. Before each experiment, a reference sample consisting of a dilute fluorescein solution was measured. The samples were imaged at 37 °C using a temperature control system consisting of an objective heater and the Stable Z specimen warmer (Bioptechs Inc., Butler, PA, USA). Images were acquired every 10 min for a period of 15 h in the experiment for three different caspases or every 15 min for 12.5 h in the experiment where all three sensors monitor caspase 3 activity.

4.4. Image processing

To correct for uneven illumination, parallel and perpendicular images were divided pixel-wise by the corresponding parallel and perpendicular images acquired from a dilute fluorescein solution. As the anisotropy value of fluorescein is close to zero, this operation also constitutes an effective G-factor correction, which corrects for differences in the detection sensitivity for the two polarization directions, which are introduced by various optical components, such as the dichroic filters [17]. In both resulting images, the background fluorescence was then estimated from the average intensity in a small area outside the cells, and subtracted, yielding the corrected parallel image ($I_{\|}$), and perpendicular image ($I_{\perp}$).

As the emission polarizers introduce a slight shift between the two images, registration artifacts will arise, visible as shadows in the anisotropy image, unless a correction is applied. The extent of the shift is the same for all data acquired and was determined by calculating the maximum agreement using 2D autocorrelation shifting the perpendicular image of a representative data set, with sub-pixel accuracy. The estimated shifts were used to correct the perpendicular image ($I_{\perp}$), before calculating anisotropy. All data analysis operations were performed in Python 3.5.2. Cell Profiler was used to segment and track cells in the acquired images to later generate curves corresponding to mean attributes ($I_{\|}$, $I_{\perp}$) of each individual cell. These were later used to calculate fluorescence anisotropy r through

$$r = \frac{I_{\|} - I_{\perp}}{I_{\|} + 2I_{\perp}}. \tag{1}$$

By fitting sigmoid curves to different windows of the anisotropy curves, we obtained parameters used to filter data corresponding to successful experiments (apoptotic cells) from those consistent with imaging or segmentation artifacts, as well as non-apoptotic cells. Aforementioned parameters were also used to select the time lapse where anisotropy was actually changing due to protease activity.

4.5. Anisotropy signal analysis

In order to derive the fraction of sensor in monomeric state, we cannot simply use the mean anisotropy but we have to account for changes in brightness detection. In the case of homoFRET, assuming both fluorescent proteins have not undergone photobleaching and are mature, the emission intensity of the dimer is twice that of the monomer, irrespective of FRET. However, in the case of a hetero-dimer, the differences in quantum yield and emission spectrum between the two means that the observed intensity depends on the fraction of monomer and the FP to FP distance in the dimer. Therefore, observed fluorescence intensity depends on the detected brightness of each fluorophore and its concentration,

$$I_M = b_{M_1} M_1 + b_{M_2} M_2 \tag{2}$$

$$I_D = (b_{M_1} + b_{M_2} + \delta b) D, \tag{3}$$

where M_1, M_2 and D correspond to each monomer and dimer

concentration, while I and b are fluorescence intensity and detected brightness, respectively. As fluorophore pairs are of different kind, their detected brightness will be different. Furthermore, as energy migrates during FRET, emission is not equivalent between fluorophores and this is taken into consideration as δb.

As biosensors are synthesized as pairs of fluorophores, we can assume $M_1 = M_2 = M$ leading to

$$I_M = (b_{M_1} + b_{M_2})M \tag{4}$$

$$I_D = (b_{M_1} + b_{M_2} + \delta b)D. \tag{5}$$

On the other hand, measured anisotropy depends on the intensity detected of each involved species

$$r = \frac{\sum_i I_i r_i}{\sum_i I_i}. \tag{6}$$

We can find an expression of m, proportion of sensor in monomeric state, in terms of anisotropy

$$m = \frac{b(r - r_d)}{r_m - r + (r - r_c)}, \tag{7}$$

where $b = (b_{M_1} + b_{M_2} + \delta b)/(b_{M_1} + b_{M_2})$ is the relative brightness of fluorophores in dimeric over monomeric state, and r_M and r_D correspond to anisotropy of the biosensor in monomeric and dimeric state respectively. Defining $\Delta b = \delta b/(b_{M_1} + b_{M_2})$, we can use $b = 1 + \Delta b$ in the calculation of the derivative of m, taking into consideration that anisotropy depends on time,

$$\dot{m} = \frac{1 + \Delta b}{r_M - r_D} \frac{\dot{r}}{\left[1 + \Delta b \frac{r - r_D}{r_M - r_D}\right]^2}. \tag{8}$$

To sum up, a proportional curve to $\dot{m}$ can be calculated through anisotropy, its derivative and its parameters. If a pair of monomers had the same detected brightness as a single dimer ($\Delta b = 0$) then the derivative of monomeric fraction would be proportional to the anisotropy derivative.

Finite differences of order 5 was implemented in order to derive anisotropy curves while minimizing noise in the derived curve. Δb was estimated from time series, by analyzing change in cell total fluorescence intensity when anisotropy changes, and fine tuned by correcting bias in timing of control experiment. Estimated values used for Δb were 0.15 for construct b, -0.15 for construct r and 0.17 for construct y.

We then calculated monomeric fraction derivative by applying Eq. (8). As monomer and dimer anisotropy varied considerably from cell to cell, the denominator was written in terms of the normalized anisotropy curve. The maximum activity time was obtained after interpolating with splines the calculated proportional curve to monomeric fraction derivative.

4.6. Biological model adaptation

A mass action law and ordinary differential equation based model developed by Albeck et al. [3] (Extrinsic Apoptosis Reaction Model V1.0) was adapted by the addition of the species corresponding to our biosensors in the different possible states (dimer, monomer, and in complex with caspase). Reaction constants were chosen to be the same as each caspase with its substrate. Other parameters of the model were also varied to explore new possibilities. Simulated sensor state curves were generated and subsequently studied to design predictors of caspase state. Anisotropy curves were also generated to evaluate and compare with the experimentally observed curves.

Furthermore, through mass action law it is clear that derivation of proportion of sensor in monomeric state will yield a curve proportional to caspase in complex with sensor, or, caspase instantaneous activity. Maximum caspase activity was defined as a robust proxy for caspase timing as it proved to be independent of sensor concentration and caspase function profile.

4.7. Experimental and model correspondence

As sensor concentration varied greatly producing important time variations within the model, simulations were made with various combinations of sensor concentration coming from latin hypercube sampling. This can be interpreted as the network perturbation caused by enzyme sequestration due to high sensor concentration. Anisotropy curves obtained from experiments and simulations were identically processed to obtain maximum activity times and study caspase time differences in both cases.

As timing between caspases differed from experimentally observed time differences, caspase network and bibliography were analyzed in pursuit of possible modifications that could recover experimental behaviour. After finding the biosensor concentration range that reproduced adequate correlation between time difference from caspase 3 to caspase 8 and caspase 3 to caspase 9, simulations were performed varying different parameters to explore the best correction. We assessed matching between simulated and observed times by generating two dimensional histograms and calculating the Pearson coefficient between corresponding bins (see Supplementary Fig. 4). Different binnings were used to see robustness of the method employed. A reduction in XIAP concentration to 10^2 proteins per cell and ligand to 10^3 per cell, as well as an increment in receptor concentration to 10^3 proteins per cell was found to be the best matching correction.

Acknowledgements

This work was supported by grants from the German Ministry of Education and Research (BMBF; FORSYS initiative, grant nr. 0315257 to P.J.V.), from the German Research Foundation (DFG GR 3848/1-1 to H.E.G.) and National Agency for Scientific and Technological Promotion (ANPCyT PICT 2014-3658).

The authors declare no competing financial interests.

Author contributions

P.L. did most of the cloning and performed the initial construct screening. A.A.C., K.C.S., P.L., Y.R. conducted the experiments and the image analysis. A.A.C. built the models and simulations and network analysis. P.I.H.B. proposed the idea to use anisotropy to detect multiple sensors. P.J.V. and H.E.G. designed the project. A.A.C and H.E.G. wrote the manuscript. All authors read the manuscript.

Summary

Three spectrally distinct anisotropy FRET-based biosensors are demonstrated by co-monitoring caspase 8, 9 and 3 activity upon apoptotic stimulus. Signal analysis together with biochemical modelling render a correlative dataset valuable for understanding signalling networks topology.

Appendix A. Supplementary data

Supplementary data associated with this article can be found in the online version at doi:10.1016/j.redox.2018.07.023.

References

[1] H. Ai, K.L. Hazelwood, M.W. Davidson, R.E. Campbell, Fluorescent protein fret pairs for ratiometric imaging of dual biosensors, Nat. Methods 5 (5) (2008) 401–403.

[2] J.G. Albeck, J.M. Burke, B.B. Aldridge, M. Zhang, D.A. Lauffenburger, P.K. Sorger, Quantitative analysis of pathways controlling extrinsic apoptosis in single cells, Mol. Cell 30 (1) (2008) 11–25.

[3] J.G. Albeck, J.M. Burke, S.L. Spencer, D.A. Lauffenburger, P.K. Sorger, Modeling a snap-action, variable-delay switch controlling extrinsic cell death, PLOS Biol. 6 (12) (2008) (1–1).

[4] B.B. Aldridge, S. Gaudet, D.A. Lauffenburger, P.K. Sorger, Lyapunov exponents and phase diagrams reveal multi-factorial control over TRAIL-induced apoptosis, Mol. Syst. Biol. 7 (1) (2014) (553–553).

[5] A.N. Bader, E.G. Hofman, J. Voortman, P.M. van Bergen en Henegouwen, H.C. Gerritsen, Homo-FRET imaging enables quantification of protein cluster sizes with subcellular resolution, Biophys. J. 97 (9) (2009) 2613–2622.

[6] P. Bastiaens, A. van Hoek, J. Benen, J. Brochon, A. Visser, Conformational dynamics and intersubunit energy transfer in wild-type and mutant lipoamide dehydrogenase from Azotobacter vinelandii. A multidimensional time-resolved polarized fluorescence study, Biophys. J. 63 (3) (1992) 839–853.

[7] W.P. Bozza, X. Di, K. Takeda, L.A.R. Rosado, S. Pariser, B. Zhang, The use of a stably expressed FRET biosensor for determining the potency of cancer drugs, PLoS ONE 9 (9) (2014) e107010.

[8] H.J. Carlson, R.E. Campbell, Genetically encoded fret-based biosensors for multiparameter fluorescence imaging, Curr. Opin. Biotechnol. 20 (1) (2009) 19–27 (Analytical biotechnology).

[9] Y. Ding, H.-w. Ai, H. Hoi, R.E. Campbell, Förster resonance energy transfer-based biosensors for multiparameter ratiometric imaging of ca2. dynamics and caspase-3 activity in single cells, Anal. Chem. 83 (24) (2011) 9687–9693.

[10] L.M. DiPilato, X. Cheng, J. Zhang, Fluorescent indicators of camp and epac activation reveal differential dynamics of camp signaling within discrete subcellular compartments, Proc. Natl. Acad. Sci. USA 101 (47) (2004) 16513–16518.

[11] C. Dolde, J. Bischof, S. Grüter, A. Montada, J. Halekotte, C. Peifer, H. Kalbacher, U. Baumann, U. Knippschild, B. Suter, A ck1 fret biosensor reveals that ddx3x is an essential activator of ck1ϵ, J. Cell Sci. 131 (2018) 1.

[12] W.B. Frommer, M.W. Davidson, R.E. Campbell, Genetically encoded biosensors based on engineered fluorescent proteins, Chem. Soc. Rev. 38 (10) (2009) 2833–2841.

[13] H.E. Grecco, S. Imtiaz, E. Zamir, Multiplexed imaging of intracellular protein networks, Cytom. Part A 89 (8) (2016) 761–775.

[14] E.A. Jares-Erijman, T.M. Jovin, FRET imaging, Nat. Biotechnol. 21 (11) (2003) 1387–1395.

[15] H. Kimura, Y. Hayashi-Takanaka, K. Yamagata, Visualization of dna methylation and histone modifications in living cells, Curr. Opin. Cell Biol. 22 (3) (2010) 412–418 (Nucleus and gene expression).

[16] K. Kominami, T. Nagai, T. Sawasaki, Y. Tsujimura, K. Yashima, Y. Sunaga, M. Tsuchimochi, J. Nishimura, K. Chiba, J. Nakabayashi, K. Koyamada, Y. Endo, H. Yokota, A. Miyawaki, N. Manabe, K. Sakamaki, In vivo imaging of hierarchical spatiotemporal activation of caspase-8 during apoptosis, PLoS ONE 7 (11) (2012) e50218.

[17] J.R. Lakowicz, Principles of Fluorescence Spectroscopy, third ed., (2006).

[18] T. Laviv, B.B. Kim, J. Chu, A.J. Lam, M.Z. Lin, R. Yasuda, Simultaneous dual-color fluorescence lifetime imaging with novel red-shifted fluorescent proteins, Nat. Methods 13 (12) (2016) 989–992.

[19] C.-W. Lin, C.Y. Jao, A.Y. Ting, Genetically encoded fluorescent reporters of histone methylation in living cells, J. Am. Chem. Soc. 126 (19) (2004) 5982–5983.

[20] K.Q. Luo, V.C. Yu, Y. Pu, D.C. Chang, Measuring dynamics of caspase-8 activation in a single living hela cell during tnfα-induced apoptosis, Biochem. Biophys. Res. Commun. 304 (2) (2003) 217–222.

[21] T. Ma, Y. Hou, J. Zeng, C. Liu, P. Zhang, L. Jing, D. Shangguan, M. Gao, Dual-ratiometric target-triggered fluorescent probe for simultaneous quantitative visualization of tumor microenvironment protease activity and pH in vivo, J. Am. Chem. Soc. 140 (1) (2017) 211–218.

[22] M. Machacek, L. Hodgson, C. Welch, H. Elliott, O. Pertz, P. Nalbant, A. Abell, G.L. Johnson, K.M. Hahn, G. Danuser, Coordination of rho gtpase activities during cell protrusion, Nature 461 (7260) (2009) 99–103.

[23] J.G. Miranda, A.L. Weaver, Y. Qin, J.G. Park, C.I. Stoddard, M.Z. Lin, A.E. Palmer, New alternately colored fret sensors for simultaneous monitoring of zn2. in multiple cellular locations, PLoS ONE 7 (11) (2012) 1–10.

[24] Y. Niino, K. Hotta, K. Oka, Simultaneous live cell imaging using dual fret sensors with a single excitation light, PLoS ONE 4 (6) (2009) 1–9.

[25] M. Offterdinger, V. Georget, A. Girod, P.I.H. Bastiaens, Imaging phosphorylation dynamics of the epidermal growth factor receptor, J. Biol. Chem. 279 (35) (2004) 36972–36981.

[26] A. Piljic, C. Schultz, Simultaneous recording of multiple cellular events by fret, ACS Chem. Biol. 3 (3) (2008) 156–160 (PMID: 18355004).

[27] R.D. Prasasya, D. Tian, P.K. Kreeger, Analysis of cancer signaling networks by systems biology to develop therapies, Semin. Cancer Biol. 21 (3) (2011) 200–206 (Why Systems Biology and Cancer?).

[28] M.A. Rizzo, D.W. Piston, High-contrast imaging of fluorescent protein {FRET} by fluorescence polarization microscopy, Biophys. J. 88 (2) (2005) L14–L16.

[29] S.W. Ryter, H.P. Kim, A. Hoetzel, J.W. Park, K. Nakahira, X. Wang, A.M.K. Choi, Mechanisms of cell death in oxidative stress, Antioxid. Redox Signal. 9 (1) (2007) 49–89.

[30] C. Schultz, A. Schleifenbaum, J. Goedhart, T.W.J. Gadella, Multiparameter imaging for the analysis of intracellular signaling, ChemBioChem 6 (8) (2005) 1323–1330.

[31] M. Silberberg, H.E. Grecco, pawFLIM: reducing bias and uncertainty to enable lower photon count in FLIM experiments, Methods Appl. Fluoresc. 5 (2) (2017) 024016.

[32] A. Squire, P.J. Verveer, O. Rocks, P.I. Bastiaens, Red-edge anisotropy microscopy enables dynamic imaging of homo-fret between green fluorescent proteins in cells, J. Struct. Biol. 147 (1) (2004) 62–69 (Recent Advances in Light Microscopy).

[33] L. Stegemann, K.C. Schuermann, C.A. Strassert, H.E. Grecco, Photofunctional surfaces for quantitative fluorescence microscopy: monitoring the effects of photogenerated reactive oxygen species at single cell level with spatiotemporal resolution, ACS Appl. Mater. Interfaces 7 (10) (2015) 5944–5949 (PMID: 25705918).

[34] O.V. Stepanenko, D.M. Shcherbakova, I.M. Kuznetsova, K.K. Turoverov, V.V. Verkhusha, Modern fluorescent proteins: from chromophore formation to novel intracellular applications, BioTechniques 51 (5) (2011) 313–318.

[35] K. Takemoto, T. Nagai, A. Miyawaki, M. Miura, Spatio-temporal activation of caspase revealed by indicator that is insensitive to environmental effects, J. Cell Biol. 160 (2) (2003) 235–243.

[36] L. Tyas, V.A. Brophy, A. Pope, A.J. Rivett, J.M. Tavaré, Rapid caspase-3 activation during apoptosis revealed using fluorescence-resonance energy transfer, EMBO Rep. 1 (3) (2000) 266–270.

[37] M. Vilar, I. Charalampopoulos, R.S. Kenchappa, A. Simi, E. Karaca, A. Reversi, S. Choi, M. Bothwell, I. Mingarro, W.J. Friedman, G. Schiavo, P.I. Bastiaens, P.J. Verveer, B.D. Carter, C.F. Ibáñez, Activation of the p75 neurotrophin receptor through conformational rearrangement of disulphide-linked receptor dimers, Neuron 62 (1) (2009) 72–83.

[38] M. Wachsmuth, C. Conrad, J. Bulkescher, B. Koch, R. Mahen, M. Isokane, R. Pepperkok, J. Ellenberg, High-throughput fluorescence correlation spectroscopy enables analysis of proteome dynamics in living cells, Nat. Biotechnol. 33 (4) (2015) 384–389.

[39] S. Warren, A. Margineanu, M. Katan, C. Dunsby, P. French, Homo-FRET based biosensors and their application to multiplexed imaging of signalling events in live cells, Int. J. Mol. Sci. 16 (12) (2015) 14695–14716.

[40] C.M. Welch, H. Elliott, G. Danuser, K.M. Hahn, Imaging the coordination of multiple signalling activities in living cells, Nat. Rev. Mol. Cell Biol. 12 (11) (2011) 749–756.

[41] X. Xu, A. Gérard, B.C. Huang, D.C. Anderson, D. Payan, Y. Luo, Detection of programmed cell death using fluorescence energy transfer, Nucleic Acids Res. 26 (8) (1998) 2034–2035.

[42] E. Zamir, P.H.M. Lommerse, A. Kinkhabwala, H.E. Grecco, P.I.H. Bastiaens, Fluorescence fluctuations of quantum-dot sensors capture intracellular protein interaction dynamics, Nat. Methods 7 (4) (2010) 295–298.